

A Figure of Merit Measuring Picture Resolution†

T. RINDFLEISCH and D. WILLINGHAM

Jet Propulsion Laboratory, Pasadena, California, U.S.A.

INTRODUCTION

The subject of resolution arises in virtually all applications of facsimile systems and particularly so for spacecraft television systems. Prior to a spacecraft mission, system and trajectory variables must be optimized with respect to expected picture quality. Clearly, the overall system resolution depends on many things including the scene properties determining contrast, image motion, atmospheric turbulence, system characteristics, and characteristics of the observer viewing the scene reproduction. It is very difficult to do laboratory resolution measurements to determine the interdependence of system resolution on all of these factors. It is nevertheless necessary to know this dependence in order to analyze and optimize system variables with respect to picture resolution. Thus the object of this paper is to calculate a figure of merit measuring the resolution of a complex facsimile system including the effects of the factors described above and to present the results in a form useful for system design and general analysis.

For extended scenes such as the Moon, a useful measure of resolution is a dimension of the smallest typical object in a scene which can be detected by an observer using the system. Normally, the scene reproduction will be a photograph displaying the scene brightness distribution degraded by loss of definition, noise, etc., and the observer is taken to be the human eye-brain system which is sensitive to brightness. Although this situation will be considered here, it is clearly not the only case of interest, since facsimile devices and observers (microphotometers or computers) can be visualized which respond to information distributions in many different ways. In any case, the observer must be capable of determining whether signal-plus-noise or simply noise is present at the output. Schade¹ has made measurements on the detectability of isolated objects displayed against uniform backgrounds and finds that a signal-to-r.m.s.-noise ratio of 3 gives a detection probability of about 80%.

† This paper presents the results of one phase of research carried out at the Jet Propulsion Laboratory, California Institute of Technology, under contract NAS 7-100, sponsored by the National Aeronautics and Space Administration.

Using this result, a figure of merit measuring picture resolution can be defined as the length of a side of the smallest uniformly bright square displayed against a uniform background which produces a signal-to-r.m.s.-noise ratio of 3 for an observer. The brightnesses of the square and its background are determined by the characteristics of the scene and lighting which produce contrast. For the Moon, these characteristics would be the illumination and viewing geometry, the surface reflectance function, and the average slope of relief features.

The problem is therefore, to calculate, as a function of size, the signal-to-r.m.s.-noise ratio produced at the observer's output when viewing the degraded reproduction of a uniform square on a uniform background.

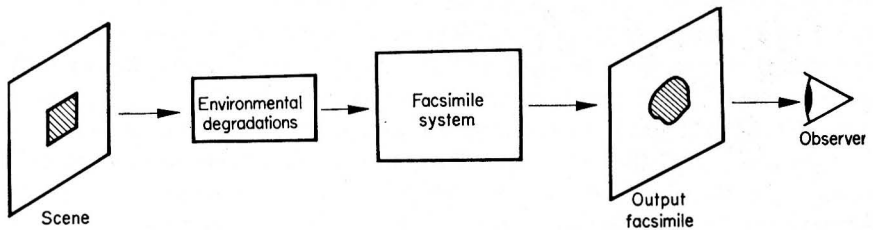


FIG. 1. Schematic diagram of facsimile process.

The calculation must account for effects due to image motion, atmospheric turbulence, and facsimile system transfer characteristics. From this result the figure of merit will be equal to the size of the square which produces a signal-to-r.m.s.-noise ratio of 3. A schematic diagram of the system to be analyzed is shown in Fig. 1.

ANALYSIS OF SYSTEM†

An attractive mathematical approach to this problem lies in the formalism of linear-system analysis. Such an approach allows many varied effects to be included in a unified and consistent manner. The assumptions made in using linear analysis are: (1) the system processes a sum of input functions as if each term of the sum were processed separately; (2) there exists a complete set of functions each of which when processed by the system is changed only in normalization (these functions are usually taken to be sine waves). The justification for applying these assumptions to practical systems usually relies on small-signal arguments which are straightforward and will not be repeated here. It should be noted that this linearity assumption is fundamental to this calculation since almost all subsequent steps rely on it.

Because of the importance of the above assumptions, a short digression on their practical application is in order. A linear facsimile system

† See p. 353 for list of symbols.

can be described by three inherent properties: (1) the uniform field transfer characteristic measuring the conversion of d.c. input amplitudes to output amplitudes; (2) the eigenfunction (sine-wave) response characteristic measuring the relative normalization degradation as a function of the eigenfunction parameter (spatial frequency); and (3) the noise power spectrum of the system appearing at the output. Clearly the second property is the most important since it enables the response of the system to an arbitrary varying input to be predicted. The fact that the response of a system to a sine-wave input is also a sine wave is not obvious *a priori* and cannot be demonstrated as in the case of

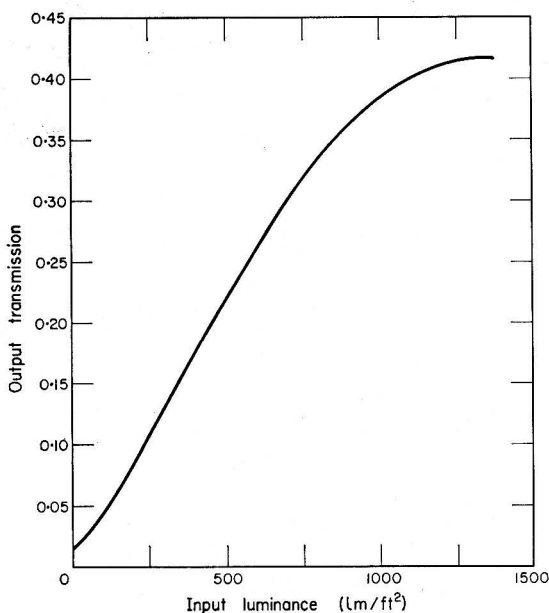


FIG. 2. Typical uniform field transfer function for a Ranger spacecraft camera system

simple electrical and mechanical systems. Whereas this point is currently being investigated in detail by the authors, at present it must be assumed that in the small-signal approximation a useful sine-wave response function exists and can be measured. The small-signal assumption imposes the use of low-contrast targets for this measurement. This requirement must be complied with when attempting a description of a complete system by this method.

Assuming that linear-system analysis provides a reasonable facsimile system description, at least in the small-signal approximation (for low contrast scenes this is a valid assumption), it is possible to calculate the

figure of merit defined earlier. (Note that measurements and examples will be taken from the Ranger series of spacecraft for which this work was originally done.) Taking the facsimile system output to be a positive film transparency, the uniform-field transfer function will be assumed to relate the output film transmittance linearly to the input brightness. Figure 2 shows a typical transfer curve for a Ranger spacecraft camera system.

For the case of a spatially varying input-brightness distribution, $b(x,y)$, the resulting output-transmittance distribution, $t(x,y)$, can easily be written down from linear analysis as

$$t(x,y) = t_0 + a \int_{-\infty}^{\infty} dk_x \int_{-\infty}^{\infty} dk_y G(k_x, k_y) B(k_x, k_y) \times \exp[i(k_x x + k_y y)], \quad (1)$$

where t_0 is a transfer constant, a is the slope of the uniform-field transfer function, (k_x, k_y) are spatial frequency components and $B(k_x, k_y)$ is the Fourier transform of $b(x,y)$, i.e.,

$$B(k_x, k_y) = \frac{1}{(2\pi)^2} \int_{-\infty}^{\infty} dx \int_{-\infty}^{\infty} dy b(x,y) \exp[-i(k_x x + k_y y)].$$

Also, $G(k_x, k_y) = G_{\text{SWR}}(k_x, k_y) \times G_{\text{MOT}}(k_x, k_y) \times G_{\text{TURB}}(k_x, k_y) \times \dots$,

where $G(k_x, k_y)$ is the effective spatial filter of the overall system and G_{SWR} , G_{MOT} , G_{TURB} , etc., are the camera system sine-wave response function, the image motion spatial filter, the atmospheric turbulence spatial filter, and other possible filtering effects. It is this part of the formulation which allows the degradation that will appear in the scene reproduction to be predicted.

The results of sine-wave response measurements on a typical Ranger spacecraft camera are shown in Fig. 3. Note that the data points have been fitted to a Gaussian curve. Clearly the system sine-wave response function will be complex for a television process. In fact, it can be shown that for a point-scanned raster the real and imaginary parts of the sine-wave response function must form a Hilbert transform pair. Figure 3 shows only the amplitude response and the associated phase shift has been neglected. Attempts to measure the phase response for the Ranger spacecraft systems have been unsuccessful since significant phase shifts do not occur until the amplitude modulation is lost in the system noise. This will be the case for most high-resolution systems and no great error is incurred by neglecting the phase shift portion of the sine-wave response function.

It is simple to show that the effects of image motion can be considered as a spatial filter. The exact response of the filter depends on the type of shutter used and on the type of motion involved. For a perfect

behind-the-lens shutter and uniform motion, it can be shown that

$$G_{\text{MOT}}(k_x, k_y) = \frac{2 \sin \mathbf{k} \cdot \mathbf{v} \delta \tau / 2}{\mathbf{k} \cdot \mathbf{v} \delta \tau},$$

where \mathbf{k} is the wave vector in the image plane, \mathbf{v} is the velocity vector in the image plane, and $\delta \tau$ is the exposure time.

Similarly the effects of atmospheric turbulence can be included as a spatial filter although it is difficult to calculate this factor accurately.

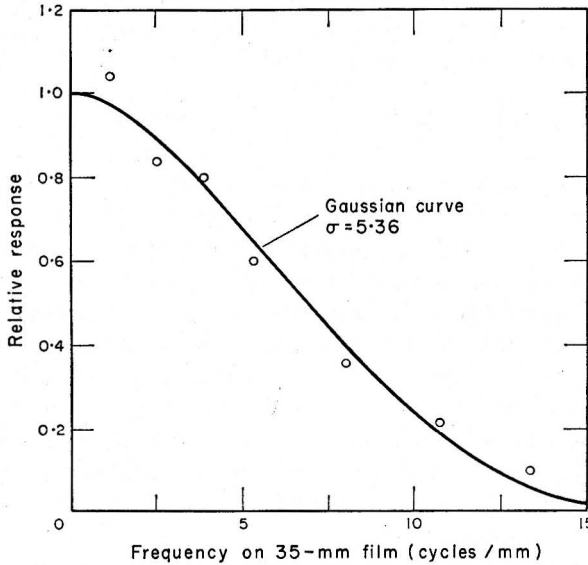


Fig. 3. Typical sine-wave response amplitude curve for a Ranger spacecraft camera.

It depends on the amount and type of turbulence present and is generally approximated by a Gaussian distribution with an appropriate half-width.

Only the maximum signal portion of Eq. (1), t_S^{max} , is of interest, and it can be shown, using the conditions that $t(x,y)$ is a real function and the phase shift is small, that

$$t_S^{\text{max}} = a \int_{-\infty}^{\infty} dk_x \int_{-\infty}^{\infty} dk_y G(k_x, k_y) B_S(k_x, k_y), \quad (2)$$

where $B_S(k_x, k_y)$ is the signal component of the Fourier transform of the input brightness distribution.

It is necessary for an observer to view the illuminated output transparency containing the signal plus system-noise and decide whether or not a signal is present. It is clear that the observer will try to optimize the viewing conditions to facilitate his decision. This optimization is

conveniently formulated by considering the observer to act as a spatial filter. This assumes that the observer acts as a linear operator, which hypothesis is difficult to test, except perhaps indirectly through the predictions of the theory. Schade² among others, has investigated the sine-wave response of the eye and concluded that it acts as a low-pass filter. Although questions have been raised as to the linearity of the eye-response³ it will be assumed here that the linear-system postulate is valid for the human observer for the small-signal case under consideration. Then if the observer can be considered as a filter whose response is $H(k_x, k_y)$ where the normalization $H(0,0)$ is arbitrary, the maximum signal at the observer's output is, from Eq. (2),

$$S_{\text{OBS}} = aI_0 \int_{-\infty}^{\infty} dk_x \int_{-\infty}^{\infty} dk_y G(k_x, k_y) H(k_x, k_y) B_S(k_x, k_y), \quad (3)$$

where I_0 is the uniform illumination intensity of the output transparency. Note that in writing down Eq. (3) it has been assumed that the observer's eye is linearly sensitive to brightness. For the human observer, since the eye is usefully sensitive over decades of brightness range, a more logarithmic dependence is implied. However, the small-signal approximation for low contrast scenes will not produce large brightness variations and to a first order approximation a linear transfer characteristic in brightness will be assumed to hold. In fact it would have been possible to assume that the uniform brightness transfer function of the camera and film is linear in film density and thereby incorporate the non-linear response of the eye. For small signals these are equivalent approaches.

All that remains to be known in order to assess the observer's output signal-to-noise ratio is the distribution of the system noise. There are many sources of noise in a television system, including electronic noise, kinescope noise, and recording film noise. For the present analysis, only the power spectrum of the resultant transmittance noise appearing in the output reproduction of a uniform input scene is important. This spectrum will be assumed wide with respect to the system bandwidth so that a "white" noise approximation is valid. It should be noted that the amplitude of the white-noise power spectrum depends on the mean transmittance of the output film, since neither a very transparent nor a very dense film exhibits much noise. It must also be pointed out that the effects of scan-line structure have been ignored. The scan lines represent a coherent multiplicative noise which appears both in the signal and noise expressions. For a densely scanned raster, however, the scan-line overlap allows one to ignore this effect. Thus if the film transmittance white-noise power spectrum has an amplitude N_0 , the r.m.s. noise at the observer's output (after observer filtering)

is given by

$$N_{\text{r.m.s.}} = I_0 \sqrt{N_0} \left[\int_{-\infty}^{\infty} dk_x \int_{-\infty}^{\infty} dk_y H^2(k_x, k_y) \right]^{1/2}. \quad (4)$$

Dividing Eq. (3) by (4), gives the signal-to-r.m.s.-noise ratio at the observer's output

$$\frac{S}{N} \Big|_{\text{OBS}} = \frac{a \int_{-\infty}^{\infty} dk_x \int_{-\infty}^{\infty} dk_y G(k_x, k_y) H(k_x, k_y) B_S(k_x, k_y)}{\sqrt{N_0} \left[\int_{-\infty}^{\infty} dk_x \int_{-\infty}^{\infty} dk_y H^2(k_x, k_y) \right]^{1/2}}. \quad (5)$$

As discussed earlier, it is assumed that the observer is able to alter the conditions of viewing so as to optimize his detection efficiency. This procedure can be formulated mathematically by equating this alteration with changing the observer filter spectrum so as to maximize the perceived signal-to-noise ratio, Eq. (5). The observer can alter his spectral response by such simple actions as magnification and defocusing or by more subtle interactions of the eye-brain system. Two mathematical models for this process will be presented differing in the latitude allowed to the observer for changing the spectrum of his filter.

The first model assumes that there is no restriction on the shape of the observer's spectral response. In this case, optimizing Eq. (5) with respect to the function $H(k_x, k_y)$ is equivalent to optimizing the expression

$$\frac{\int_{-\infty}^{\infty} dk_x \int_{-\infty}^{\infty} dk_y G(k_x, k_y) H(k_x, k_y) B_S(k_x, k_y)}{\left[\int_{-\infty}^{\infty} dk_x \int_{-\infty}^{\infty} dk_y H^2(k_x, k_y) \right]^{1/2} \left[\int_{-\infty}^{\infty} dk_x \int_{-\infty}^{\infty} dk_y G^2(k_x, k_y) B_S^2(k_x, k_y) \right]^{1/2}}.$$

Applying Schwarz's inequality in a straightforward manner shows that the maximum value occurs for

$$H(k_x, k_y) = G(k_x, k_y) B_S(k_x, k_y),$$

thus giving for the optimized observer signal-to-r.m.s.-noise ratio

$$\frac{S}{N} \Big|_{\text{max}} = \frac{a}{\sqrt{N_0}} \left[\int_{-\infty}^{\infty} dk_x \int_{-\infty}^{\infty} dk_y G^2(k_x, k_y) B_S^2(k_x, k_y) \right]^{1/2}. \quad (6)$$

The maximum output signal-to-r.m.s.-noise ratio of the observer's model is thus calculable from Eq. (6) by finding the integral of the squared product of the sine-wave response of the system and the signal spectrum of the uniform square on a uniform background as a function of the square dimension. Then setting $S/N|_{\text{max}} = 3$ for threshold detectability, the figure of merit equal to the corresponding square size can be obtained.

This is a somewhat clumsy process to go through for an analysis of the complete system. It is useful therefore to investigate the dependence of Eq. (6) on the detailed shape of $G(k_x, k_y)$ for a fixed $B_S(k_x, k_y)$. It will be assumed that $G(0,0) = 1$ always. There are two limiting cases of interest.

(1) The spectrum of $G(k_x, k_y)$ is much wider than $B_S(k_x, k_y)$ so that over the range that $B_S(k_x, k_y)$ extends $G(k_x, k_y) \approx G(0,0) = 1$, then

$$\frac{S}{N}\Big|_{\max} \approx \frac{a}{\sqrt{N_0}} \left[\int_{-\infty}^{\infty} dk_x \int_{-\infty}^{\infty} dk_y B_S^2(k_x, k_y) \right]^{1/2}.$$

(2) The spectrum of $B_S(k_x, k_y)$ is much wider than $G(k_x, k_y)$ so that

$$\frac{S}{N}\Big|_{\max} \approx \frac{a}{\sqrt{N_0}} B_S(0,0) \left[\int_{-\infty}^{\infty} dk_x \int_{-\infty}^{\infty} dk_y G^2(k_x, k_y) \right]^{1/2}.$$

Thus the maximum signal-to-r.m.s.-noise ratio is independent of $G(k_x, k_y)$ in case (1). In case (2) equal signal-to-r.m.s.-noise ratios result for sine-wave response characteristics having equal integrals of $G^2(k_x, k_y)$ in the limits $\pm \infty$. This suggests a common width definition for all sine-wave response functions such that

$$\int_{-\infty}^{\infty} dk_x \int_{-\infty}^{\infty} dk_y G^2(k_x, k_y) = 4\sigma^2. \quad (7)$$

Then all response characteristics with the same σ value yield asymptotically equal signal-to-r.m.s.-noise ratios for an optimized observer in this model. This width definition is equivalent to the N_e definition proposed by Schade⁴ in analogy to the electrical case.

Considering only equivalent response functions as defined by Eq. (7) irrespective of detailed shape, the figure of merit resulting from Eq. (6) can be evaluated in the two asymptotic regions. The signal spectrum for a uniform square on a uniform background is

$$B_S(k_x, k_y) = \frac{\Delta b \sin k_x l/2 \sin k_y l/2}{\pi^2 k_x k_y}, \quad (8)$$

where Δb is the luminance difference between the square and the background and l is the length of a side of the square. Thus using the detectability criterion, $S/N|_{\max} = 3$, the figure of merit, which is equal to the corresponding square size l , is given by:

(1) the spectrum of $G(k_x, k_y)$ much wider than $B_S(k_x, k_y)$, ($\sigma l \gg 1$),

$$\sigma l \approx \frac{6\pi\sigma\sqrt{N_0}}{a\Delta b}; \quad (9)$$

(2) the spectrum of $B_S(k_x, k_y)$ much wider than $G(k_x, k_y)$, ($\sigma l \ll 1$),

$$\sigma^2 l^2 \approx \frac{6\pi^2\sigma\sqrt{N_0}}{a\Delta b}. \quad (10)$$

Note that the problem naturally breaks into dimensionless parameters.

Now the transition region ($\sigma l \approx 1$) must be investigated. Clearly the results in this region depend upon the detailed response shape but fortunately not in a sensitive manner. At this point, to facilitate calculations, it will be assumed that $G(k_x, k_y) = G(k_y, k_x)$. Assuming that $G(0,0) = 1$, Eq. (6) is used to evaluate $S/N|_{\max}$ for a variety of response fall-off characteristics. Figure 4 shows five fall-off shapes representative of those investigated. These range from an exponential fall-off to a rectangular fall-off. Note that phase shifts have been neglected except for the $\sin x/x$ case and all of the plotted curves have $\sigma = 1$.

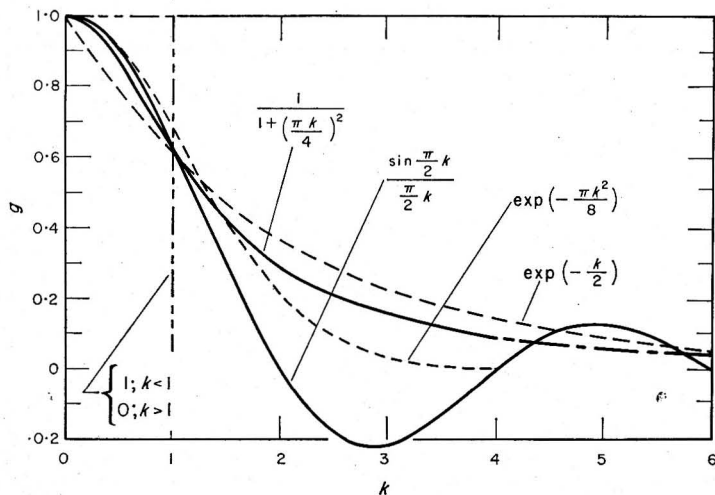


FIG. 4. Response curves for typical filter shapes.

Figure 5 then shows the results of calculating the figure of merit in the transition region ($\sigma l \approx 1$) for these shapes. Note that only the boundaries of the region containing the resulting curves are shown since this is the point of interest. The axes represent the parameters resulting from the asymptotic analysis. An average curve could be drawn which lies within 10% of either boundary. One would like to infer that this is quite a general result, i.e., the curve for any reasonable fall-off characteristic between the rectangular and exponential functions should lie within the boundaries in Fig. 5.

The above results rely on a model which perhaps allows too much latitude to the observer to shape his filter in order to optimize the output signal-to-noise ratio. An alternative and more restrictive approach would be to assume the observer filter to be of a given shape but with variable width. The observer then adjusts this width to optimize his output signal-to-noise ratio.

The mathematics for this observer model can be formulated as follows. Equation (5) still gives the basic expression for the observer's output signal-to-noise ratio. If σ_{OBS} is the width of the observer filter $H(k_x, k_y)$ (in the sense of Eq. (7)), Eq. (5) is solved for the figure of merit under the optimization conditions

$$\left. \frac{S}{N} \right|_{\text{OBS}} = 3,$$

and

$$\frac{\partial}{\partial \sigma_{\text{OBS}}} \left. \frac{S}{N} \right|_{\text{OBS}} = 0. \quad (11)$$

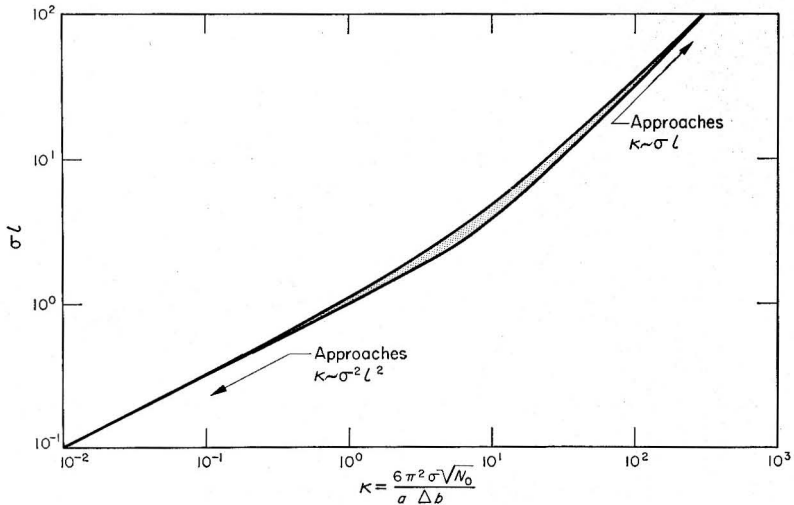


FIG. 5. Results obtained for the figure of merit assuming an optimized detection system.

This model is even clumsier than the first, but here again the resulting figure of merit might not be sensitive to the detailed filter shapes. Under the same filter symmetry assumptions as earlier, one can calculate the figure of merit for the filter shapes shown in Fig. 4 under the conditions in Eq. (11). Now one filter must be chosen for the system response function and one for the observer. The boundaries of the results for the twentyfive cases are shown in Fig. 6. The problem produces the same dimensionless quantities appearing along the axes. Note there is a somewhat wider dispersion than in Fig. 5 but still an average curve can be drawn lying within 15% of the boundaries.

The dispersion at the asymptotes results from the fact that an observer with a given spectral response may or may not act as an optimum observer. In this regard the lower boundary in Fig. 6 is identical with the lower boundary in Fig. 5. Again one would like to

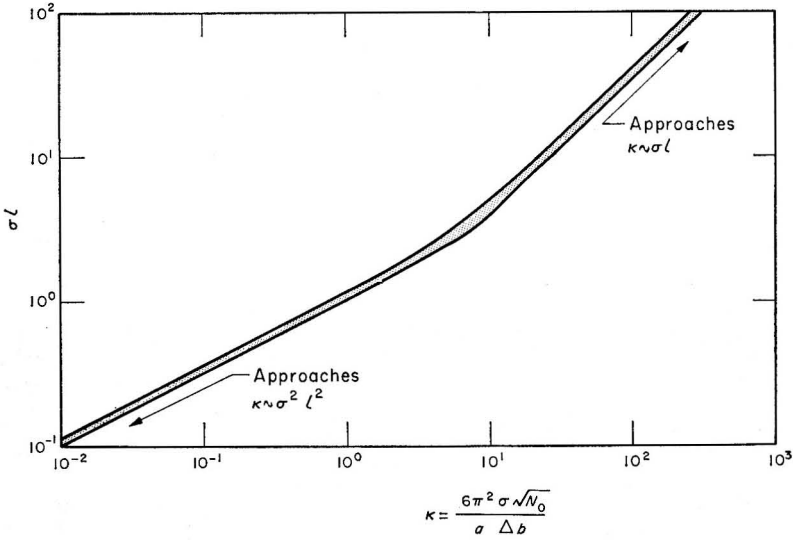


FIG. 6. Figure of merit for an observer acting as a low-pass band filter.

infer that any reasonable fall-off characteristic lying between the exponential and rectangular functions will give a figure of merit curve within these boundaries.

Figure 7 shows a single curve half-way between the boundaries of Fig. 6. This curve agrees with the theory to within 15% and within the filter shape range considered.

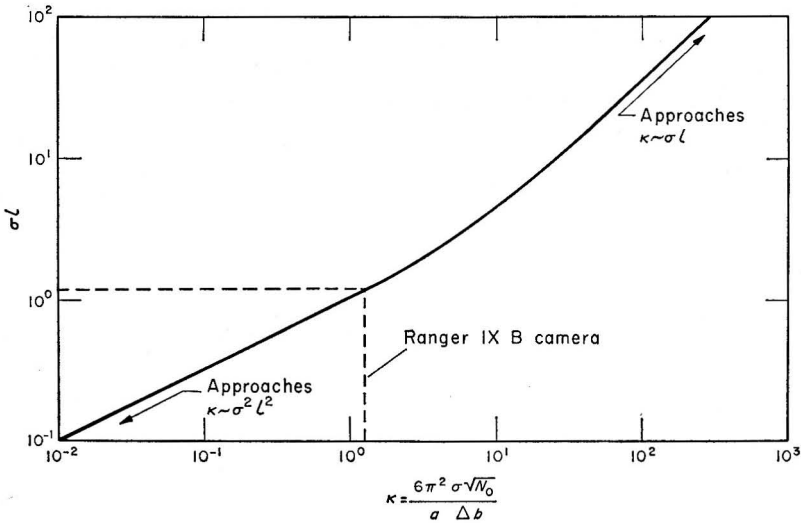


FIG. 7. Average figure of merit.

EXPERIMENTAL TESTS

The final question to be considered relates to the accuracy of the theory. Clearly many assumptions have gone into the analysis presented, the most important of which allowed the application of linear analysis. In general this assumption limits the analysis to a first order theory in the small-signal region. This in turn limits it to low contrast scenes. The Moon indeed satisfies this criterion. Thus the pictures obtained by the Ranger spacecraft cameras provide a test of the theory. Pictures



FIG. 8. Calculated figure of merit for a frame of a camera mounted on the Ranger IX spacecraft.

from the three Ranger missions offer a test over a range of about one order of magnitude of the variable $\kappa = 6\pi^2\sigma\sqrt{N_0}/a\Delta b$. In Fig. 7 the data for a Ranger IX B camera frame are shown. The necessary calibration measurements were made before the flight and the scene contrast was found from the lunar reflectance function and the viewing geometry for an assumed 15° slope (taken from radar measurements). The resulting figure of merit is slightly less than twice the scan-line spacing and is shown in Fig. 8, in which the square at the point of the

arrow has sides equal to the figure of merit. It must be remembered that the picture in Fig. 8 has gone through several generations of reproduction since the original for which the calibration data apply. The figure of merit as calculated measures the resolution limits of the picture quite well. This can be verified by viewing the same area in a later frame at better resolution.

Using the Ranger frames to verify the theory is very tedious although useful. A careful test of the theory is being undertaken by the authors using laboratory arrangements in which the variables can be well controlled. These measurements include testing the limits of applicability of linear-system analysis. No final results are yet available as only preliminary measurements have been made.

CONCLUSIONS

A first order theory has been presented which allows, by means of a single curve (Fig. 7) and standard calibration data, the prediction of the resolution capabilities of a complex system. Within this formulation the effects of image motion, atmospheric turbulence, scene contrast, system sine-wave response, system noise, and the limitations in response of the observer, are accounted for in a unified manner, all these parameters being considered as effective spatial filters. Clearly if it were possible to measure in sufficient detail the resolution capabilities of the system under consideration in its intended operational environment, there would be no need for the present analysis. However, if this is impossible as in the case of spacecraft missions, the present formulation would prove very useful.

REFERENCES

1. Schade, O. H., "An Evaluation of Photographic Image Quality", *RCA Electron Tube Division*, EM-7752, December 14, 1962.
2. Schade, O. H., *RCA Rev.* **9**, 5 (1948).
3. Bryngdahl, O. *Optica Acta* **12**, 1 (1965).
4. Schade, O. H., *J. Soc. Motion Picture Televis. Engrs* **58**, 181 (1952).

NOMENCLATURE

a	Uniform field transfer function slope
$b(x, y)$	Input scene brightness distribution
$B(k_x, k_y)$	Fourier transform of $b(x, y)$
$B_S(k_x, k_y)$	Signal portion of $B(k_x, k_y)$
$G(k_x, k_y)$	Composite system sine-wave response function
$G_{\text{SWR}}(k_x, k_y)$	Facsimile system sine-wave response function
$G_{\text{MOT}}(k_x, k_y)$	Effective image motion spatial filter
$G_{\text{TURB}}(k_x, k_y)$	Effective atmospheric turbulence spatial filter
$H(k_x, k_y)$	Effective observer spatial filter
I_0	Output transparency illumination intensity

(k_x, k_y)	Spatial frequency components
\mathbf{k}	Wave vector with components k_x and k_y
l	Uniform target square dimension
N_0	Amplitude of white transmittance noise power spectrum
$N_{r.m.s.}$	Root-mean-square noise amplitude at observer's output
N_e	Equivalent band-pass as defined by Schade ⁴
S_{OBS}	Signal at observer's output due to t_S^{\max}
$S/N _{OBS}$	Signal-to-r.m.s.-noise ratio at observer's output
$S/N _{\max}$	Optimized signal-to-r.m.s.-noise ratio at observer's output
$t(x, y)$	Output film transmittance distribution
t_0	Base film transmittance
t_S^{\max}	Spatially maximized transmittance signal at output film
\mathbf{v}	Image motion velocity vector at output film
(x, y)	Coordinates in output film transparency
$\delta\tau$	Exposure time
Δb	Brightness difference between uniform square and background in an input scene
κ	A variable equal to $6\pi^2\sigma\sqrt{N_0}/a\Delta b$
σ	Response function width parameter, in the sense defined by Eq. (7)
σ_{OBS}	Width parameter for the effective observer filter in the same sense as σ